Polarity in oxide ultrathin films

2008 J. Phys.: Condens. Matter 20 264003

(http://iopscience.iop.org/0953-8984/20/26/264003)

J. Phys.: Condens. Matter **20** (2008) 264003 (10pp) doi:10.1088/0953-8984/20/26/264003

Polarity in oxide ultrathin films

Claudine Noguera and Jacek Goniakowski

CNRS, UMR7588, INSP, Campus Boucicaut, 140 rue de Lourmel, Paris 75015, France
and
Université Pierre et Marie Curie-Paris 6, UMR7588, INSP, Paris 75015, France

Received 19 November 2007, in final form 9 January 2008
Published 9 June 2008
Online at stacks.iop.org/JPhysCM/20/264003

Abstract
Relying on first-principles calculations within density functional theory and on an analytical model for the electronic structure, we present an overview of specific electronic and structural features of polar ultrathin films. MgO(111) unsupported films of finite thickness are chosen as a generic system, in order to extract general concepts associated with polarity at the nanoscale, relate them to the well-known semi-infinite case, and unravel specific scenarios of polarity compensation which are not present for the latter. Size dependent behavior of the compensating charge and formation energy, changes in crystallographic structure, and the possibility of substantial lattice distortions throughout entire films are analyzed and discussed.

(Some figures in this article are in colour only in the electronic version)

1. Introduction

Polarity has become an increasingly active research area in the field of oxide surfaces [1, 2] because it yields original surface configurations (large cell reconstructions, faceting) on which atoms are in a peculiar environment and display an electronic structure far from the usual. Indeed, accumulation of alternating layers of oppositely charged ions produces a macroscopic polarization and a surface energy which increase linearly with thickness [3]. In practice, polar surfaces are always compensated. This means that the electrostatic divergence is healed by the presence of additional (compensating) surface charges, which quench the macroscopic dipole, assure a finite surface energy, and thus stabilize the entire stacking.

For ultrathin films, on the other hand, things may be drastically different. First, it is not *a priori* obvious that polarity represents an energy handicap, as long as the thickness remains small. Indeed, a nanometric insulator can in principle sustain a non-null polarization along a polar axis. In addition, there may exist other strategies for circumventing polarity, possibly involving all layers in the films, whenever the penetration lengths of the surface electrostatic and elastic perturbations are of the order of the film thickness. In this context, it is striking that polarity in finite size systems has been the subject of rather few studies and that general concepts have not yet emerged. There have been attempts to produce clean, stoichiometric, and unreconstructed (111) films of MnO [4], NiO [5], MgO [6–8], FeO [9, 10], CoO [11, 12], NaCl [13], or (0001) films of ZnO [14–16]. Observations of unreconstructed MgO(111) films on Ag(111) [6], FeO(111) films on Pt(111) [10, 17], NaCl(111) films on Al(111) [18] and ZnO films on Ag(111) [16] suggest that none of the mechanisms of compensation at work in semi-infinite systems are present.

We have recently undertaken a systematic study of model ultrathin unsupported MgO(111) films, using *ab initio* simulation methods [19, 20, 22]. The density functional method at the PW-91 gradient-corrected level [23] was used, with ultrasoft pseudopotentials [24], and corrections for the residual dipole, as implemented in VASP [25]. The systems were represented by a slab geometry, with a (1×1) two-dimensional (2D) unit cell, with a void thickness at least equal to 10 Å. As regards stoichiometric films, we have shown that there exist low energy configurations which involve either a complete change of the oxide atomic structure (hexagonal boron nitride B_k structure, rather than B1 rock-salt) or an absence of compensating charges at the surface (strongly distorted B3 zinc-blende structure). With the aim of going one step further towards the understanding of the growth of thin MgO(111) films, this study is extended to non-stoichiometric configurations presenting an excess of one complete magnesium or oxygen layer. The geometries under consideration are depicted in figure 1. We stress that the objects in the limit of large N thickness always have a *finite* thickness, with *two* (possibly different) terminations, characteristics of thin film geometry.

Here, we present an overview of these results and we support the numerical findings with an analytical model which

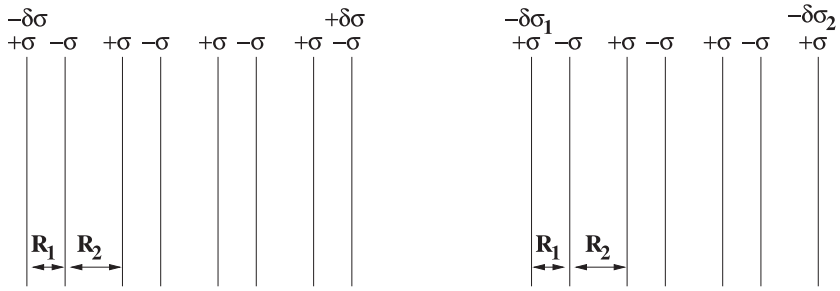

Figure 1. Capacitor model for stoichiometric (left) and non-stoichiometric (right) films. In the first case, the first and Nth bilayers correspond to cation and anion terminations, respectively. In the right panel, an excess of one cation layer is represented as an incomplete $(N + 1)$th bilayer. Successive interlayer distances are labeled R_1 and R_2. In the analytical model, charge modifications $\delta\sigma$, $\delta\sigma_1$ and $\delta\sigma_2$ are assumed to take place only on the outermost layers.

accounts for the main characteristics of the electronic degrees of freedom, in both stoichiometric and non-stoichiometric systems. We emphasize that our focus is not on the behavior of *actual* MgO thin films, since the approximations made—unsupported films and a (1×1) 2D unit cell—are somewhat restrictive. We rather try to extract general concepts associated with polarity at the nanoscale, and unravel specific scenarios of polarity compensation which are not present for semi-infinite systems.

The paper successively considers the limits of large (sections 2 and 3) and small (section 4) thicknesses. The relative stabilities of the various configurations are discussed in section 5.

2. Large thickness regime: stoichiometric films

Thick polar films are expected to behave very similarly to semi-infinite surfaces, and be compensated by charge modifications in the surface regions. Such processes are well documented for stoichiometric semi-infinite systems. In numerical simulations, the limit of large thickness has often been considered, in order to mimic semi-infinite surfaces. Results can be found in the literature on MgO(111), ZnO(0001), ZrO_2 [26–28], which indicate how the $N \rightarrow \infty$ limit is reached. However, for systems with an excess of one cationic or anionic layer, to our knowledge, no systematic study exists. In this section, we analyze the characteristics of MgO(111) films grown in a rock-salt (B1) or zinc-blende (B3) geometry, which are among the competitive structures for the structural ground state (see section 5). We first summarize the results obtained for stoichiometric films, and then interpret them with a simplified electronic structure model. A similar approach is developed in the next section for non-stoichiometric films.

The film thickness is quantified by the number N of formula units (MgO bilayers) in the (1×1) unit cell. Successive interlayer distances are labeled R_1 and R_2, with $R_2 = 3R_1$ for the B3 structure and $R_1 = R_2$ for the B1 structure (figure 1). We recall that, in the $N \rightarrow \infty$ limit, whatever the mechanism of compensation, the electrostatic condition for counterbalancing the macroscopic dipole moment requires that charge reduction $\delta\sigma_\infty = \sigma R_1/(R_1 + R_2)$ is present on the outer layers on each side of the film.

2.1. Numerical results

The main numerical results can be summarized as follows:

- The shortest interlayer distances R_1 present a systematic reduction with respect to their bulk values; the ratio $R_1/(R_1 + R_2)$ smoothly converges towards the bulk values 0.5 and 0.25 for the B1 and B3 structures, respectively.
- The formation energies (computed as the difference between the film energy and the energy of its constituents when embedded in their respective bulk structures) tend towards a constant value as $N \rightarrow \infty$ with an approximate $1/N$ behavior. As displayed in figure 2 for B1(111) films, the $1/N$ slope is larger when relaxation effects are included than for rigid geometries.
- The surface electronic configuration is 'metallic', with a partially filled CB on the magnesium outer layer and a partially depleted VB on oxygen outer layers, as sketched in the right panel of figure 2. Indeed, partial filling of surface bands is the only mechanism of polarity compensation consistent with the present computational set-up (complete atomic layers and a (1×1) 2D unit cell).
- As a result, the outermost layers present a reduction of charge $\delta\sigma$, with respect to the charge density σ at the film center, which converges towards the expected $N \rightarrow \infty$ limit: $\delta\sigma_\infty = \sigma R_1/(R_1 + R_2)$ with an approximate $1/N$ behavior. Again, the $1/N$ slope is larger when relaxation effects are included (figure 2). Charges have been estimated by integration of the valence electronic density in Voronoi cells [29] and $\delta\sigma$ is systematically calculated as the result of charge modifications in the two outermost layers.
- There exists a residual jump of potential Φ across the films of the order of the bulk gap (e.g. 4.1 versus 3.6 eV for B3(111) films and 3.1 versus 4.6 eV for B1(111) films in rigid geometry). That these values do not increase linearly with N is a sign of polarity compensation.

2.2. Analytical model

In order to formally assess these results, we present a tight binding self-consistent model for the electronic structure of such films, assuming a rigid geometry (constant R_1 and R_2 throughout the film) and charge modifications $\delta\sigma$ only on the

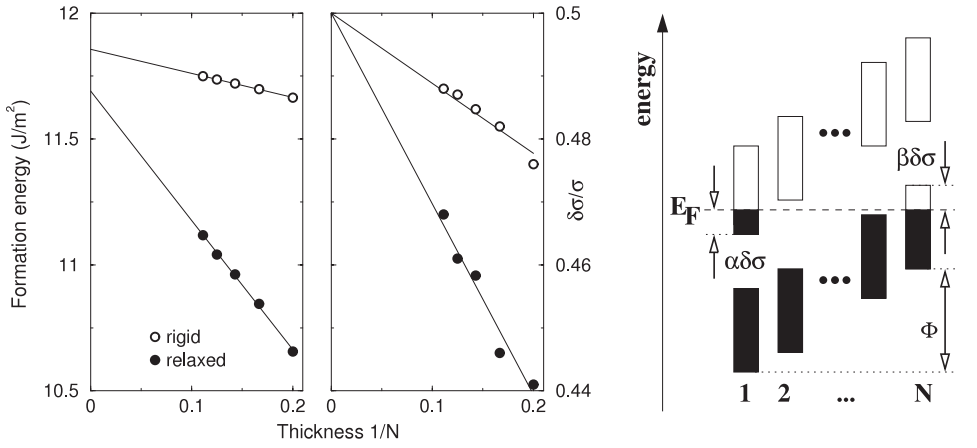

Figure 2. Left panels: formation energy of B1(111) stoichiometric films and compensating charge $\delta\sigma/\sigma$ as a function of $1/N$ for unrelaxed (open symbols) and relaxed (filled symbols) geometries. Right panel: sketch of the film band structure. Filled and empty electronic states are represented in black and white, respectively. $E_{\rm F}$ denotes the Fermi level. See the text for details.

outermost layers. In the following, the indexes A and C refer to anion and cation species, respectively. Atomic units are used throughout; $e = \hbar = m = 1$.

The electrostatic potential which acts on the various layers n includes two long range contributions: one due to the (unmodified) charge densities $\pm\sigma$, and the other due to the compensating charge density $\pm\delta\sigma$. Associated with the latter, there is a potential correction, due to intra-atomic electron–electron interactions ($U_{\rm A}$ and $U_{\rm C}$ are the intra-atomic Coulomb matrix elements and A is the 2D unit cell area) on the outer layers:

$$\begin{aligned} V_{\rm C1} &= -AU_{\rm C}\delta\sigma \\ V_{{\rm C}n} &= -4\pi\sigma R_1(n-1) + 4\pi\delta\sigma(R_1+R_2)(n-1) \\ V_{{\rm A}n} &= -4\pi\sigma R_1 n + 4\pi\delta\sigma(n(R_1+R_2) - R_2) \\ V_{{\rm A}N} &= -4\pi\sigma R_1 N + 4\pi\delta\sigma(N(R_1+R_2) - R_2) + AU_{\rm A}\delta\sigma. \end{aligned} \tag{1}$$

V thus displays a linear decrease across the film, with a slope equal to $-4\pi\sigma R_1 + 4\pi\delta\sigma(R_1+R_2)$, plus an anomaly on the outer layers due to intra-atomic Coulomb interactions. It bends the bands so that, in a rigid band approximation, the bottom of the conduction band (CBm) and the top of the valence band (VBM) for the nth layer are shifted to local values equal to

$$\mathrm{CBm}_n = \mathrm{CBm}^0 - V_{{\rm C}n} \qquad \mathrm{VBM}_n = \mathrm{VBM}^0 - V_{{\rm A}n}. \tag{2}$$

To enable a charge density modification $\delta\sigma$, the Fermi level has to intersect the surface valence and conduction bands in such a way that they are partially depleted and filled (figure 2, right panel). Assuming constant densities of states in the CB and VB ($1/\alpha$ and $1/\beta$, respectively), the equalization of the Fermi level yields

$$E_{\rm F} = \mathrm{CBm}_1 + \alpha\delta\sigma = \mathrm{VBM}_N - \beta\delta\sigma. \tag{3}$$

The value of $\delta\sigma$ results:

$$\delta\sigma = \frac{4\pi N R_1\sigma - G}{4\pi N(R_1+R_2) + \widetilde{V}} \tag{4}$$

with $\widetilde{V} = A(U_{\rm A}+U_{\rm C}) + \alpha + \beta - 4\pi R_2$ and $G = \mathrm{CBm}^0 - \mathrm{VBM}^0$. As expected, when N tends to infinity, $\delta\sigma$ converges towards $\delta\sigma_\infty = \sigma R_1/(R_1+R_2)$.

The bands are shifted with respect to one another in the successive bilayers, as represented in figure 2 (right panel). The total shift across the film is equal to

$$\Phi = V_{\rm C1} - V_{{\rm A}N} = G + (\alpha+\beta)\delta\sigma. \tag{5}$$

This potential drop represents the energy difference between the HOMO on the right side of the film and the LUMO on the other side, which has to be overcome in order to enable $\delta\sigma$. It is of the order of the gap width G plus an additional term due to bandwidth effects. Even in the thermodynamic limit, it never vanishes: its absolute value $\Phi_\infty = G + (\alpha+\beta)\delta\sigma_\infty$ represents the remainder of the polarity perturbation once charge compensation $\delta\sigma_\infty$ has been produced by surface band metalization. This quantity plays a central role in the film energetics and size dependence effects.

When $N \to \infty$, the band shift between two successive layers Φ/N becomes negligibly small, which allows a quasi-'bulk' electronic structure to be achieved in the central part of the film. In this limit, $\delta\sigma$ may be written as

$$\delta\sigma \approx \delta\sigma_\infty - \frac{\Phi_\infty\epsilon^\infty}{4\pi d} + \cdots \tag{6}$$

with $d = N(R_1+R_2)$ the film thickness, and ϵ^∞ the optical dielectric constant. It can be shown that higher order terms in the development are also proportional to $\Phi_\infty\epsilon^\infty$. This development is consistent with our numerical results in rigid geometry (figure 2). The first-order correction is also consistent with the electrostatic model proposed in [27, 28], but in addition, the present model gives an explicit, albeit approximate, expression for the optical dielectric constant:

$$\epsilon^\infty = \frac{G + \widetilde{V}\delta\sigma_\infty}{G + (\alpha+\beta)\delta\sigma_\infty}. \tag{7}$$

For large gap insulators (G much larger than both Coulomb $\widetilde{V}\sigma$ and bandwidth $(\alpha+\beta)\sigma$), screening is inefficient and $\epsilon^\infty \to 1$

as expected. For moderate gap values and small bandwidths, an insulating type of screening is recovered: $\epsilon^\infty \approx 1 + \widetilde{V}\delta\sigma_\infty/G$ with short range (the U terms) and long range Coulomb interactions competing in $\widetilde{V}$ and a denominator proportional to the gap width [30]. It should be noted that neglecting intra-atomic Coulomb terms yields negative screening ($\epsilon^\infty < 1$). For metals ($G \to 0$), $\epsilon^\infty \to \widetilde{V}/(\alpha+\beta)$, which means that better screening is obtained for larger bandwidths. Equation (7) is thus general enough to account for screening in all types of materials, whatever the relative values of the gap, the bandwidth and Coulomb forces.

There are two distinct energy terms associated with polarity: the electrostatic energy $E_{\rm el}$ which involves the polarization energy term and intra-atomic Coulomb repulsion, and the change in band filling $E_{\rm B}$. Per 2D surface cell area, they amount to

$$E_{\rm el} = 2\pi N R_1 \sigma(\sigma - \delta\sigma) - 0.5\delta\sigma(G + (\alpha+\beta)\delta\sigma) - 0.5\sigma\delta\sigma(U_{\rm A} + U_{\rm C})A \qquad (8)$$

$$E_{\rm B} = G\delta\sigma + 0.5(\alpha-\beta)\delta\sigma^2.$$

In the large N limit, as shown in the appendix, with $\delta\sigma$ given by equation (4), the term proportional to N, issuing from $E_{\rm el}$, yields the bulk electrostatic energy. The term independent of N is a contribution to the cleavage energy. It involves a term $\Phi_\infty\delta\sigma_\infty$ which is likely to be dominant in large gap insulators, and corresponds to the transfer of $\delta\sigma_\infty$ electrons through the gap (figure 2). This term is larger in wide gap insulators (large G values), in strongly ionic systems (large σ) and in structures with large $R_1/(R_1+R_2)$ ratios (B1(111) orientation for example). The *total* cleavage energy, on the other hand, also involves bond breaking contributions (narrowing of the bands at the surface), which should be taken into account when comparing with experimental or numerical values, but are not included in the present model. The energy term proportional to $1/N$ in the large N limit tells how the macroscopic limit is reached. Like $\delta\sigma$, it is proportional to the quantity $\Phi_\infty\epsilon^\infty$. When relaxation effects are included, the static dielectric constant ϵ_0 (zero-frequency limit) has to be used instead of ϵ^∞. This explains the systematically larger slopes found numerically when relaxation effects are included ($\epsilon_0 > \epsilon^\infty$). The expression for the $1/N$ term is in agreement with previous estimations which neglected bandwidth and Coulomb U terms [27, 28] and with the numerical results given in section 2.1. This shows that the macroscopic limit is smoothly reached.

To summarize, when they are stoichiometric, thick polar films present electronic properties which are very close to those of semi-infinite stoichiometric polar surfaces, with partially filled bands and compensating charges on their outermost layers. The film energetics and the strength of the size dependence effects are mainly determined by the remainder of the polarity perturbation $\Phi_\infty = G + (\alpha+\beta)\delta\sigma_\infty$ and by the dielectric function of the material.

3. Large thickness regime: non-stoichiometric films

Before presenting a similar description for neutral films involving an excess of one atomic layer, we draw attention to the electrostatic condition for cancelation of the macroscopic dipole in a geometry such as the one depicted in figure 1 (right panel), with one excess anion or cation layer, in the limit $N \to \infty$. Indeed, it is much less widely recognized that, in the general case of $R_1 \neq R_2$, such a condition implies that charge reductions on the two opposite sides of the film have to be different and given by $\delta\sigma_1 = \sigma R_1/(R_1+R_2)$ and $\delta\sigma_2 = \sigma R_2/(R_1+R_2)$, whatever the mechanism of compensation.

3.1. Numerical results

The results can be summarized as follows:

- The ratio $R_1/(R_1+R_2)$ remains practically constant as thickness increases for B1(111) films, while it increases smoothly towards the bulk value for B3(111) films (e.g. in the presence of cation excess: 0.22 at $N = 3$, 0.23 at $N = 5$, expected value 0.25 at $N \to \infty$).
- The formation energy with respect to the corresponding bulks and free atoms tends smoothly towards its $N \to \infty$ limit in a quasi-$1/N$ fashion. However, the slope is much smaller than for stoichiometric films, and it nearly vanishes for the B1 rigid geometry (figure 3, for films with cation excess).
- The surface electronic configuration is metallic, with a partially filled CB on both magnesium outer layers for films with a magnesium excess, as sketched in the right panel of figure 3. For films with oxygen in excess, the valence band is partially depleted on both oxygen outer layers.
- The residual jump of potential through the films is close to 0.6 eV for B3 films (much lower than when the films are stoichiometric) and zero for B1 ones.
- The outermost layers present reductions of charge densities $\delta\sigma_1$ and $\delta\sigma_2$ which approach the limits $\sigma R_1/(R_1+R_2)$ and $\sigma R_2/(R_1+R_2)$ in a quasi-$1/N$ fashion (figure 3). For B3 films, the $1/N$ slope is smaller than when they are stoichiometric; for B1 films, it is quasi-null. For films with oxygen in excess, the charge modification is not as localized as is the case for magnesium terminations. This gives a hint that oxygen–oxygen hybridization is substantial.

For B3(111) films with an excess of one oxygen layer, we have found two possible surface configurations. In the less stable one, the oxygens adsorb close to bulk-like sites. The structural and charge configurations are analogous to those found for an excess of one magnesium layer. In the more stable configuration, the oxygen atoms bind to the underlying oxygen layer, forming charged O_2 groups, which bear the compensating charge. In both cases, total charge reductions of $\approx 0.75\sigma$ and $\approx 0.25\sigma$ are recovered on the opposite sides of the films, with very small, if any, variation with thickness.

It should be noted that the characteristics of the 'large thickness regime' that we have just described are found down to thicknesses equal to $N = 4$ for B3(111) and down to $N = 2$ for B1(111) non-stoichiometric films.

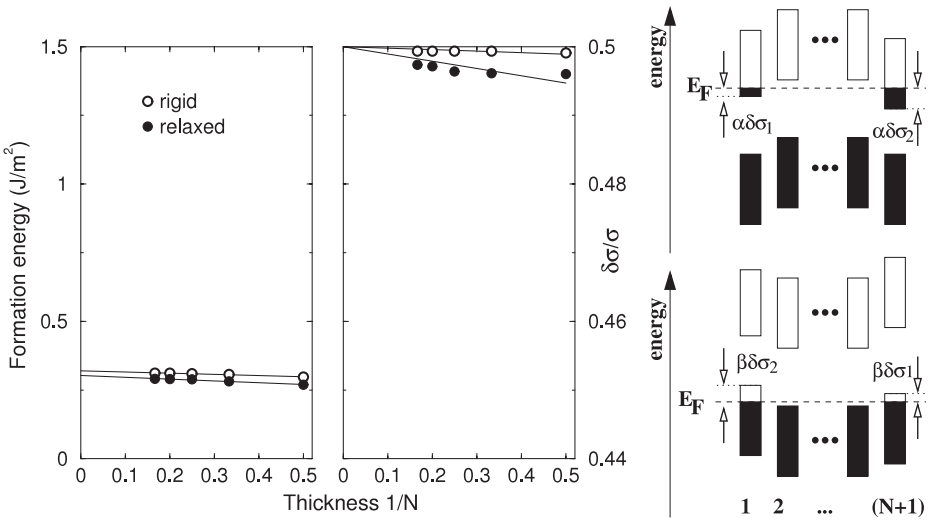

Figure 3. Left panels: formation energy and compensating charge $\delta\sigma/\sigma$ for B1(111) films with an excess of one magnesium layer, as a function of $1/N$ for unrelaxed and relaxed geometries. In order to emphasize the large difference in variation of these two quantities as a function of $1/N$, as compared to the stoichiometric films, the scales are identical to those in figure 2. Right panel: sketch of the band structure in the case of magnesium (top) and oxygen (bottom) excess. Filled and empty electronic states are represented in black and white, respectively. E_F denotes the Fermi level.

3.2. Analytical model

We now present an analytical description of the electronic structure, along the same lines and with the same basic assumptions as in section 2. To be specific, we restrict the following discussion to films with cations in excess. We assume that the charge distribution departs from $\pm\sigma$ only on the two outermost cationic layers, by amounts $\delta\sigma_1$ and $\delta\sigma_2$ on the left and right sides of the film, respectively (figure 1). Charge neutrality requires that $\delta\sigma_1+\delta\sigma_2=\sigma$. The expressions for the electrostatic potential throughout the film are identical to those in equation (1) with $\delta\sigma$ replaced by $\delta\sigma_1$, except on the outermost layer:

$$V_{C(N+1)} = -4\pi\sigma R_1 N + 4\pi\delta\sigma_1 N(R_1+R_2) - AU_C\delta\sigma_2. \quad (9)$$

The Fermi level intersects the two conduction bands on the outer cationic layers (assumed to have the same bandwidth $1/\alpha$). Its equalization yields

$$E_F = \mathrm{CBm}_1 + \alpha\delta\sigma_1 = \mathrm{CBm}_{N+1} + \alpha\delta\sigma_2 \quad (10)$$

from which $\delta\sigma_1$ and $\delta\sigma_2$ may be deduced:

$$\delta\sigma_1 = \frac{4\pi N R_1\sigma + \widetilde{V}\sigma}{4\pi N(R_1+R_2)+2\widetilde{V}}$$
$$\delta\sigma_2 = \frac{4\pi N R_2\sigma + \widetilde{V}\sigma}{4\pi N(R_1+R_2)+2\widetilde{V}} \quad (11)$$

with $\widetilde{V} = AU_C + \alpha$. When $R_1 = R_2$, i.e. for B1 films, the charge modification is independent of thickness and $\delta\sigma_1 = \delta\sigma_2 = \sigma/2$. When this is not the case, as expected, $\delta\sigma_1$ converges towards $\delta\sigma_\infty = \sigma R_1/(R_1+R_2)$ and $\delta\sigma_2$ towards $\sigma - \delta\sigma_\infty$, as $N\to\infty$.

The potential jump across the film is equal to

$$\Phi = V_{C1} - V_{C(N+1)} = \alpha(\delta\sigma_2 - \delta\sigma_1). \quad (12)$$

It is thus the difference in filling of the two conduction bands, associated with the inequivalence of R_1 and R_2, which represents the remainder of the polarity perturbation. It is null for B1 films, in agreement with numerical results. The convergence of $\delta\sigma_1$ towards $\delta\sigma_\infty$ is given by the same equation (6) as for stoichiometric films. However, the potential jump $\Phi_\infty = \alpha(\sigma - 2\delta\sigma_\infty)$ is different and the optical dielectric constant ϵ^∞ in the present case is given by

$$\epsilon^\infty = \frac{\widetilde{V}}{\alpha}. \quad (13)$$

This expression is similar to that deduced from equation (7) in the limit of zero gap (and taking into account the difference in band fillings). It truly accounts for metallic screening, ϵ^∞ increasing as the density of states at Fermi level (here given by $1/\alpha$) increases. Compared to the case for stoichiometric films, in which the electrostatic perturbation was large, the thickness dependent part of $\delta\sigma_{1,2}$ turns out to be very small, and even null for B1 films.

The expressions for the electrostatic and band energy terms associated with polarity are parallel to those written in section 2.2. They read

$$E_{el} = 2\pi N R_1\sigma(\sigma - \delta\sigma) - 0.5\alpha\delta\sigma_1(\delta\sigma_2 - \delta\sigma_1) - 0.5\sigma\delta\sigma_1 U_C A$$
$$E_B = 0.5\alpha(\delta\sigma_1^2 + \delta\sigma_2^2). \quad (14)$$

The contribution to the cleavage energy (term independent of N) involves band terms and a Coulomb U term, but, for non-stoichiometric films, the gap width G does not enter its expression (cf the appendix). As for stoichiometric films, the

$1/N$ term is proportional to $\Phi_\infty \epsilon^\infty$. Since, as discussed above, Φ_∞ only contains band terms, it is much smaller than for stoichiometric films (and even zero for B1 films), consistently with numerical findings.

To summarize, non-stoichiometry in thick polar films yields partially filled bands and charge reduction on the outermost layers. This would also be the case for non-polar films. However, polarity requires that the electron excess (or depletion) be distributed in a well-defined way on the outer layers (equation (11)), in order to cancel the macroscopic polarization. For structures with $R_1 \neq R_2$, charge reductions $\delta\sigma_1$ and $\delta\sigma_2$ are different on the two sides of the films and the remainder of the polarity perturbation $\alpha(\delta\sigma_2 - \delta\sigma_1)$ is proportional to the difference $R_2 - R_1$. It does not involve the gap width and is thus much weaker than for stoichiometric films (actually null for B1 films). As a result, the thickness dependent part of the compensating charges and of the film formation energy is particularly small.

4. Low thickness regime

In the preceding sections we have described the characteristics of thick films in which polarity is compensated by charge redistribution. In the low thickness regime, the situation may be drastically different, since there is no macroscopic polarization to counterbalance. In previous studies [19, 20], we have found that two quite general alternative scenarios may arise in stoichiometric films, leading to structural and/or electronic properties which are strongly size dependent and peculiar with respect to thick films or semi-infinite surfaces. Here, we present these results in a wider context, which includes films containing an excess of one oxygen or magnesium layer.

4.1. New structural ground state

The first scenario involves the stabilization of a structural ground state different from the bulk one for the entire film. The driving force is the possibility of avoiding polarity by changing the layer structure, thus lowering the electrostatic contribution to the formation energy.

We have shown that in stoichiometric MgO(111) films, the lowest energy phase consistent with the hexagonal environment is the graphitic-like $B_k(0001)$ structure, met in hexagonal boron nitride (h-BN), rather than the expected rock-salt B1 bulk structure [19]. Although in the bulk, the B_k structure is less stable by 0.06 eV/MgO unit than the B1 one, its (0001) surface is non-polar, made of six member rings with equal numbers of magnesiums and oxygens. Its cleavage energy is thus much lower than that of the polar B1(111) phase and the B_k to B1 transition may be considered as driven by surface effects. The latter become insufficient for stabilizing the B_k structure when thickness increases. It was shown in [19] that this result provides a consistent interpretation of recent experimental findings [6, 7]. The same graphitic-like phase was also predicted to be the ground state of unsupported polar ultrathin films of compounds with a wurtzite bulk structure, such as ZnO, AlN, BeO, GaN, SiC and ZnS [14, 15], and was recently observed for ZnO(0001) films by means of surface x-ray diffraction [16]. A similar scenario, involving a structural transformation throughout the entire film, has been predicted also for ultrathin polar $ZrO_2(110)$ films [21].

The non-polar character of $B_k(0001)$ films is preserved in the presence of an excess magnesium layer. The excess magnesiums form a quasi-neutral metallic layer, weakly bound to the underlying surface. The situation is qualitatively similar in the presence of an oxygen excess, but the surface adsorption is reinforced by the formation of surface peroxyl groups. As a consequence, the outermost surface layer becomes a neutral O–Mg–O peroxide trilayer, of nearly zero dipole moment. Adsorption of molecular oxygen on the $B_k(0001)$ surface (not compatible with the constraint of a (1×1) surface unit cell used in the present study) will be discussed elsewhere [22].

4.2. Uncompensated polarity

The second scenario involves the stabilization of a strongly distorted structure for the entire film, for which atomic displacements reduce the polarization to such an extent that polarity compensation is no longer required.

Metastable distorted B3(111) films of various iono-covalent compounds may indeed remain polar and uncompensated over a non-negligible range of film thicknesses (in the case of MgO, up to four MgO layers) [20]. This is made possible thanks to a considerable reduction of the R_1 interplanar distance ($R_1/(R_1+R_2) \approx 0.02$) with respect to the bulk B3 value ($R_1/(R_1+R_2) = 0.25$), while ionic charges remain quasi-bulk-like. The uncompensated polar character results in unusual and strongly thickness dependent properties: the formation energy, the electronic gap, and the total dipole moment vary linearly with the film thickness N; figure 4.

The layers may thus be seen as an association of capacitors, with charge densities $\pm\sigma$ on their plates, and a total dipole moment $P_{\text{tot}} = N\sigma R_1$ proportional to N. Neglecting local environment effects (short range part of the electrostatic potential), the bottom of the conduction band (CBm) and the top of the valence band (VBM) are shifted in successive layers by an amount

$$\begin{aligned} \text{CBm}_n &= \text{CBm}^0 + 4\pi\sigma R_1(n-1) \\ \text{VBM}_n &= \text{VBM}^0 + 4\pi\sigma R_1 n \end{aligned} \tag{15}$$

as depicted in figure 4. For small N values, the jump of potential across the film $\Phi(N) = 4\pi N\sigma R_1$ is insufficient to make the valence and conduction bands overlap. The films thus remain insulating with a total gap $G(N) = G - 4\pi\sigma R_1 N$ which decreases linearly with the film thickness and no charge transfer occurs between the surface bands.

For *non-stoichiometric* B3(111) films, the situation changes drastically. In the presence of a magnesium excess, the uncompensated regime completely disappears: the films display modified surface charges and a closed gap as described in section 3. This may be associated with the small energetic cost of polarity compensation by the metal/oxide (Mg/MgO) interface [32].

In the presence of oxygen excess, there exists an uncompensated polar state only for $N = 3$. The atomic

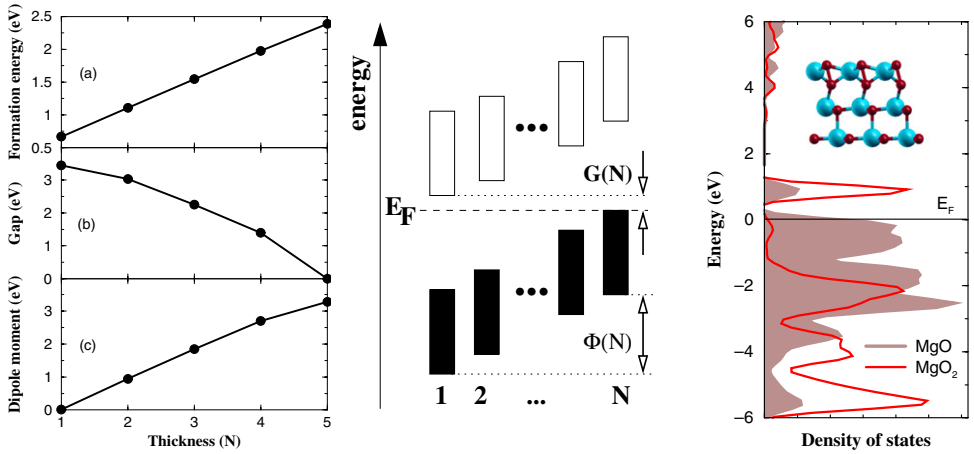

Figure 4. Left panel: thickness dependence of the formation energy, the electronic gap, and the total dipole moment for uncompensated stoichiometric polar B3(111) films. Middle panel: sketch of the corresponding band structure. Right panel: density of states of an $N = 3$ uncompensated B3(111) film with an excess oxygen layer. The LDOS on the MgO_2 surface groups (in red) displays an insulating character and some hybridization with the bands in the underlying layers (gray continuum). Inset: side view of the film structure; small (red) balls and large (blue) balls refer to oxygen and magnesium atoms, respectively.

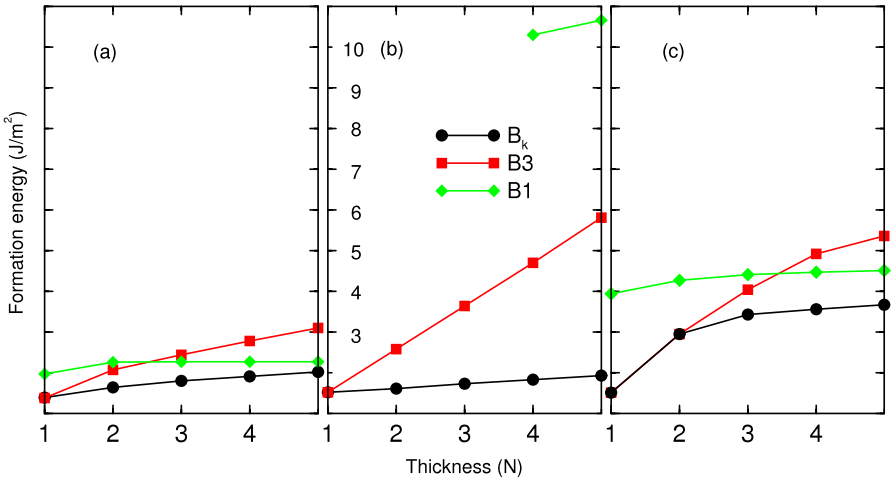

Figure 5. Formation energies of MgO B1(111), B3(111), and B_k(0001) ultrathin films as a function of film thickness N. Energies of stoichiometric (middle panel), magnesium rich (left panel), and oxygen rich (right panel) films are referred to B1 bulk MgO, atomic Mg and O. The energy scales of the three panels have been shifted so as to align the ground state energies at $N = 1$.

structure consists of two strongly distorted MgO bilayers (with very small $R_1/(R_1 + R_2)$ as in the stoichiometric case) beneath an O–Mg–O peroxide trilayer (figure 4, right panel). The electronic gap is open and the surface charges are bulk-like, except in the peroxo group O_2^{2-}. Beyond $N = 3$, a polar compensated state is restored, as described in section 3, while below $N = 3$, films spontaneously relax towards the B_k phase.

In summary, there exist two generic scenarios specific to polar films at low thickness. On the one hand, films may adopt an atomic structure, different from the bulk one, for which their orientation is non-polar. This scenario, met in the B_k(0001) films, holds for both stoichiometric and non-stoichiometric MgO films over a wide range of thicknesses. On the other hand, as long as their thickness remains below a critical value, polar films may sustain an uncompensated polarity thanks to a lattice distortion which reduces considerably their total dipole moment. This scenario, encountered for the 'flattened' B3(111) films, holds for stoichiometric films up $N \approx 4$, but becomes marginal for the non-stoichiometric ones.

5. Energetics

The present section discusses the energetics of thin polar films whether stoichiometric or with an excess of magnesium or oxygen layer. Figure 5 displays energy diagrams, in which all formation energies are calculated with respect to B1 bulk MgO. Oxygen and magnesium atomic energies are the additional references for non-stoichiometric configurations. We will restrict ourselves to a comparison of the relative stabilities of different configurations at a fixed stoichiometry. The complete analysis of the overall stability as a function of chemical environment which requires us to

work in the grand canonical ensemble will be discussed elsewhere [22].

In the following, we focus on the two most striking characteristics of figure 5. First, regardless of stoichiometry and of film thickness, the B_k structure is always found to be the most stable. Second, the B1(111) formation energy, which is considerable for stoichiometric films, is greatly reduced when oxygens or magnesiums are is excess in such a way that the B1 structure may become competitive with the other two. A similar effect, although less pronounced, is observed for B3(111) films.

For each of the three stoichiometries considered, the graphitic-like B_k structure happens to be the ground state. This can be assigned principally to its non-polar character. Indeed, adsorption of an additional magnesium or an oxygen layer does not significantly alter the overall structure of the films, nor their non-polar character. Conversely, the polar character of stoichiometric B1(111) and B3(111) films is preserved upon adsorption of excess magnesium or oxygen. At this point, it may be useful to recall that the (1×1) symmetry imposed in the present calculations disables polarity compensation by non-stoichiometric reconstructions. These latter will be considered elsewhere [22].

The formation energies of stoichiometric films in the three structures considered are significantly different and reflect the respective strengths of polarity effects. Indeed, the energy ordering of the three configurations reflects the values of $\Phi_\infty \delta\sigma_\infty$ (section 2.2) and thus follows the ratios $R_1/(R_1+R_2)$. $B_k(0001)$ films are the most stable with $R_1/(R_1+R_2) = 0$; for B3(111) films, $R_1/(R_1+R_2) \to 0.25$, while the B1(111) films are the least stable with $R_1/(R_1+R_2) \approx 0.5$.

Conversely, for non-stoichiometric films, the formation energies of the three structures are closer to each other. For example, B1(111) films are only about 1 J m^{-2} higher in energy than $B_k(0001)$ ones, while the corresponding difference amounts to nearly 10 J m^{-2} when they are stoichiometric. We note that this energy reduction depends little on the nature of the excess layer. It is thus not driven by the peculiarities of magnesium or oxygen bonding, but rather reflects differences in the way the compensating charges $\delta\sigma$ are obtained.

Indeed, for B1 and B3 stoichiometric films, $\delta\sigma$ results from electron redistribution between the valence and conduction bands and thus requires electronic promotion across the gap. The cost in energy is of the order of $G\delta\sigma$ (equation (18)), as compared to non-polar B_k films. Indeed, the difference in formation energy of B1 and B_k films in the non-stoichiometric and stoichiometric cases (about 9 J m^{-2}) corresponds to the total energy difference of about 3.5 eV per 2D unit cell, and is comparable to the DFT gap value of bulk MgO. A similar argument holds for B3(111) films but with a reduced $\delta\sigma$ and a somewhat smaller gap. Considering the systematic underestimation of DFT band gaps, such differences of formation energies are likely to be somewhat underestimated. However, the ordering just described will not be qualitatively changed.

For non-stoichiometric films, whether polar (B1 and B3) or non-polar (B_k), the valence band is partly depleted (oxygen excess) or the conduction band partly filled (magnesium excess). What differentiates polar from non-polar films is the way electrons (resp. holes) are spatially distributed and fill the conduction (resp. valence) band. This is a much more subtle effect than that for stoichiometric films, where electron promotion through the gap does (B1 and B3) or does not (B_k) take place. The energy differences between non-stoichiometric structural phases are accordingly much smaller.

In summary, the relative stabilities of various structures in ultrathin films may drastically depend upon the film stoichiometry. While regardless of stoichiometry, the non-polar $B_k(0001)$ phase is the structural ground state, the energy dispersion among B1(111), B3(111), and $B_k(0001)$ structures is significantly enhanced in the stoichiometric films. We assign this effect to an additional energy cost due to electron transfer across the band gap, necessary for polarity compensation in the latter.

6. Conclusion

Relying on first-principles calculations within DFT and on an analytical model for the electronic structure, we have presented an overview of specific electronic and structural characteristics that ultrathin polar films may display, in order to circumvent polarity. We have chosen MgO(111) unsupported films of finite thickness as a generic system in order to extract general concepts associated with polarity at the nanoscale, and unravel specific scenarios of polarity compensation which do not arise for semi-infinite systems.

We have shown that thick polar films present electronic properties which are very close to those of semi-infinite stoichiometric polar surfaces, with partially filled bands and compensating charges distributed in a well-defined way on the outer layers, in order to cancel the macroscopic polarization. The way the $N \to \infty$ limit is reached is a function of the remainder of the polarity perturbation Φ_∞ and of the dielectric constant of the material. For stoichiometric films, Φ_∞ is large and involves the gap width, while for films with an excess magnesium (resp. oxygen) layer, it is much smaller and only amounts to the difference in CB (resp. VB) filling between opposite sides of the film.

At low thickness, there exist two generic scenarios specific to stoichiometric polar films. On the one hand, they may adopt an atomic structure, different from that of the bulk, for which their orientation is non-polar (e.g. $B_k(0001)$). On the other hand, up to a critical thickness, the films may adopt a strongly distorted polar structure (e.g. B3(111)) which reduces their total dipole moment, and thus may accommodate an uncompensated polarity without surface charge modification. However, this uncompensated state becomes marginal in the presence of an excess magnesium or oxygen layer. Such thin non-stoichiometric films recover the characteristics of the large thickness regime.

The relative stability of alternative structures in ultrathin films may drastically depend upon the film stoichiometry. We have shown that, regardless of stoichiometry, the non-polar $B_k(0001)$ phase is the structural ground state, while the energy dispersion among B1(111), B3(111), and $B_k(0001)$ structures is significantly enhanced in the stoichiometric films.

It is clear that a thorough understanding of polar thin film behavior is not yet reached. Besides the effective pressure that it exerts on the films, the presence of a substrate can yield other possibilities of polarity compensation, through interfacial charge transfers, for example. The temperature and environment conditions under which the films are grown may also favor non-stoichiometric reconstructions within the layers (which were not considered here). However, we thought it necessary to first firmly establish the basic concepts of nanoscale polarity and its relation to the known semi-infinite case for the simplest possible film configurations.

Acknowledgment

Support from the French ANR under project 'SIMINOX' ANR-06-NANO-009-01, is acknowledged.

Appendix

Here, using the analytical model presented in sections 2.2 and 3.2, we give the full expressions for the development of the electrostatic $E_{\rm el}$ and band energies $E_{\rm B}$ of stoichiometric and non-stoichiometric films of large thickness (large N limit).

For stoichiometric films, they amount to

$$E_{\rm el} = 2\pi N R_1 \sigma(\sigma - \delta\sigma) - 0.5\delta\sigma(G + (\alpha+\beta)\delta\sigma) - 0.5\sigma\delta\sigma(U_{\rm A} + U_{\rm C})A \qquad (16)$$

$$E_{\rm B} = G\delta\sigma + 0.5(\alpha - \beta)\delta\sigma^2.$$

In the large N limit, with $\delta\sigma$ given by equation (4), we develop $E = E_{\rm el} + E_{\rm B}$ as $E = NE_0 + E_1 + E_2/N + \cdots$. The term proportional to N yields the bulk electrostatic energy:

$$NE_0 = 2\pi N \frac{R_1 R_2}{R_1 + R_2}\sigma^2. \qquad (17)$$

E_1 is a contribution to the cleavage energy. With $\Phi_\infty = G + (\alpha+\beta)\delta\sigma_\infty$, it reads

$$E_1 = \Phi_\infty\delta\sigma_\infty - 0.5(\alpha+3\beta)\delta\sigma_\infty^2 - 0.5\delta\sigma_\infty(\sigma - \delta\sigma_\infty)(U_{\rm A} + U_{\rm C})A - 2\pi R_2\delta\sigma_\infty^2. \qquad (18)$$

The energy term proportional to $1/N$ makes use of the derivatives of $\delta\sigma$ with respect to $1/N$ and is thus proportional to $\Phi_\infty\epsilon^\infty$ (equation (7)). With $d = N(R_1 + R_2)$ the film thickness, it reads

$$E_2/N = -\frac{\Phi_\infty\epsilon^\infty}{8\pi d}(\Phi_\infty - 4\beta\delta\sigma_\infty - (\sigma - \delta\sigma_\infty)(U_{\rm A} + U_{\rm C})A - 4\pi R_2\delta\sigma_\infty). \qquad (19)$$

The equivalent derivation for magnesium in excess films yields

$$E_{\rm el} = 2\pi N R_1\sigma(\sigma - \delta\sigma) - 0.5\alpha\delta\sigma_1(\delta\sigma_2 - \delta\sigma_1) - 0.5\sigma\delta\sigma_1 U_{\rm C}A \qquad (20)$$

$$E_{\rm B} = 0.5\alpha(\delta\sigma_1^2 + \delta\sigma_2^2).$$

The E_0 term is identical to that in equation (17). The two other terms read

$$E_1 = 0.5\Phi_\infty(\sigma - 2\delta\sigma_\infty) + \alpha\delta\sigma_\infty^2 - U_{\rm C}A\delta\sigma_\infty(\sigma - \delta\sigma_\infty)$$

$$E_2/N = -\Phi_\infty\epsilon^\infty\left(\Phi_\infty - 4\alpha\delta\sigma_\infty + U_{\rm C}A(\sigma - 2\delta\sigma_\infty)\right)/8\pi d \qquad (21)$$

with $\Phi_\infty = \alpha(\sigma - 2\delta\sigma_\infty)$ and ϵ^∞ given by equation (13).

References

[1] Noguera C 2000 *J. Phys.: Condens. Matter* **12** R367 and references therein
[2] Goniakowski J, Finocchi F and Noguera C 2008 *Rep. Prog. Phys.* **71** 016501
[3] Tasker P W 1979 *J. Phys. C: Solid State Phys.* **12** 4977
[4] Rizzi G A, Petukhov M, Sambi M, Zanoni R, Perriello L and Granozzi G 2001 *Surf. Sci.* **482–485** 1474
[5] Caffio M, Cortigiani B, Rovida G, Atrei A and Giovanardi C 2004 *J. Phys. Chem.* B **108** 9919
Stanescu S, Boeglin C, Barbier A and Deville J-P 2004 *Surf. Sci.* **549** 172
Hagendorf C, Shantyr R, Neddermeyer H and Widdra W 2006 *Phys. Chem. Chem. Phys.* **8** 1575
[6] Kiguchi M, Entani S, Saiki K, Goto T and Koma A 2003 *Phys. Rev.* B **68** 115402
[7] Arita R, Tanida Y, Entani S, Kiguchi M, Saiki K and Aoki H 2004 *Phys. Rev.* B **69** 235423
[8] Xue M and Guo Q 2007 *J. Chem. Phys.* **127** 054705
[9] Ranke W, Ritter M and Weiss W 1999 *Phys. Rev.* B **60** 1527
[10] Rienks E D L, Nilus N, Rust H P and Freund H J 2005 *Phys. Rev.* B **71** 241404
[11] Entani S, Kiguchi M and Saiki K 2004 *Surf. Sci.* **566–568** 165
[12] Shantyr R, Hagendorf C and Neddermeyer H 2004 *Thin Solid Films* **464/465** 65
[13] Hebenstreit W, Schmid M, Redinger J, Podloucky R and Varga P 2000 *Phys. Rev. Lett.* **85** 5376
[14] Claeyssens F, Freeman C L, Allan N L, Sun Y, Ashfold M N R and Harding J H 2005 *J. Mater. Chem.* **15** 139
[15] Freeman C L, Claeyssens F, Allan N L and Harding J H 2006 *Phys. Rev. Lett.* **96** 066102
[16] Tusche C, Meyerheim H L and Kirschner J 2007 *Phys. Rev. Lett.* **99** 026102
[17] Berdunov N, Mariotto G, Balakrishnan K, Murphy S and Shvets I V 2006 *Surf. Sci.* **600** L287
[18] Hebenstreit W, Schmid M, Redinger J, Podloucky R and Varga P 2000 *Phys. Rev. Lett.* **85** 5376
[19] Goniakowski J, Noguera C and Giordano L 2004 *Phys. Rev. Lett.* **93** 215702
[20] Goniakowski J, Noguera C and Giordano L 2007 *Phys. Rev. Lett.* **98** 205701
[21] Añez R, Sierraalta A and Sautet P 2007 *J. Phys. Chem.* **111** 8314
[22] Goniakowski J and Noguera C 2008 in preparation
[23] Perdew J P and Wang Y 1992 *Phys. Rev.* B **41** 13244
[24] Vanderbilt D 1990 *Phys. Rev.* B **41** 7892
[25] Kresse G and Hafner J 1993 *Phys. Rev.* B **47** 558
Kresse G and Furthmüller J 1996 *Phys. Rev.* B **54** 11169
[26] Meyer B 2004 *Phys. Rev.* B **69** 045416
[27] Kresse G, Dulub O and Diebold U 2003 *Phys. Rev.* B **68** 245409
[28] Eichler A and Kresse G 2004 *Phys. Rev.* B **69** 045402
[29] Henkelman G, Arnaldsson A and Jónsson H 2006 *Comput. Mater. Sci.* **36** 254

Sanville E, Kenny S D, Smith R and Henkelman G 2007 *J. Comput. Chem.* **28** 899

[30] Noguera C 1996 *Physics and Chemistry at Oxide Surfaces* (Cambridge: Cambridge University Press)

[31] Savariault J-M and Lehmann M S 1980 *J. Am. Chem. Soc.* **102** 1298

[32] Goniakowski J and Noguera C 1999 *Phys. Rev.* B **60** 16120
Goniakowski J and Noguera C 2002 *Phys. Rev.* B **66** 85417